Bull Volcanol (2013) 75:738
DOI 10.1007/s00445-013-0738-x

COLLECTION: MONOGENETIC VOLCANISM

Modeling thickness variability in tephra deposition

Emily Kawabata · Mark S. Bebbington · Shane J. Cronin · Ting Wang

Received: 5 November 2012 / Accepted: 9 June 2013 / Published online: 2 August 2013

Abstract The attenuation of tephra fall thickness is most commonly estimated after contouring isolated and often irregular field measurements into smooth isopachs, with varying degrees of subjectivity introduced in the process. Here, we present an explicit description of the variability introduced into a semiempirical tephra attenuation relation. This opens the way to fitting models to actual tephra observations through maximum likelihood estimation, rather than using weighted least-squares estimation on the isopachs. The method is illustrated for small-scale basaltic explosive eruptions using a simple, but typical, data set of the actual tephra thickness data published from the 1973 Heimaey eruption. Of the distributions considered to describe variability in these measurements, the lognormal performed poorly, due to its tendency to predict a small number of greatly over-thickened deposits. The Weibull and gamma distributions fitted the data to a very similar degree and produced very similar estimates for the "effective volume," mean wind direction, and mass/thickness attenuation rate. The latter can be inverted to obtain an estimate of the mean column height. The estimated wind direction, and the column height derived from the estimated thickness attenuation parameter, agreed very well with the direct observations made during the eruption. Augmented by a mixture framework allowing for the incorporation of multiple lobes and/or vents, the model was able to identify the source and direction of tephra deposition for the 1977 Ukinrek Maars eruptions from only the tephra thickness data.

Keywords Tephra · Ukinrek Maars · Aleatory uncertainty · Statistical method

Editorial responsibility: I.E.M. Smith, Guest Editor

This paper constitutes part of a topical collection:

Smith IEM, Nemeth K, and Ross P-S (eds) Monogenetic volcanism and its relevance to the evolution of volcanic fields.

E. Kawabata
Institute of Fundamental Sciences–Statistics,
Massey University,
Private Bag 11222, Palmerston North 4442, New Zealand
e-mail: e.kawabata@massey.ac.nz

M. S. Bebbington (✉) · S. J. Cronin
Volcanic Risk Solutions,
Massey University,
Private Bag 11222, Palmerston North 4442, New Zealand
e-mail: m.bebbington@massey.ac.nz

S. J. Cronin
e-mail: s.j.cronin@massey.ac.nz

T. Wang
Department of Mathematics and Statistics,
University of Otago,
P.O. Box 56, Dunedin 9054, New Zealand
e-mail: Ting.Wang@otago.ac.nz

Introduction

One of the major hazards associated with explosive eruptions is the dispersal of tephra. Apart from the hazard to aviation from fine particles suspended in the upper atmosphere (Miller and Casadevall 2000), tephra hazards are associated with its deposited depth, loading, grain size, and electromagnetic and chemical properties. Tephra fall may cause respiratory illness, damage to buildings and storm-water infrastructure, render roads impassable, disable electrical distribution networks, contaminate water supplies, destroy crops, kill livestock, and drastically change landscape stability and flood vulnerability (Baxter et al. 1981; Heiken et al. 1995; Cronin et al. 1998; Stewart et al. 2006).

Tephra falls may blanket many tens to thousands of square kilometers with deposit geometry typically established by spot analysis of thickness (or mass) and other properties at individual sites. Rapid local redeposition of tephra via fluvial and aeolian processes is common and, along with compaction, means that considerable measurement error can be introduced, increasing with time from deposition. The spot tephra thicknesses are used to construct isopach maps, with interpolation typically carried out by hand drawing or increasingly by GIS interpolation methods. Isopachs (contours of ash thickness) are, in turn, the basis, along with grain-size distribution, for the most widely applied empirical methods used for estimation of volcanic eruption properties and hazard (i.e., total erupted volume, eruption column height, and mass ejection rate; Carey and Sparks 1986; Sparks 1986; Pyle 1989; Fierstein and Nathenson 1992; Bonadonna et al. 1998; Sparks et al. 1997; Pyle 2000; Sulpizio 2005). These all involve application of a mathematical function representing tephra attenuation along its longest axis, indexed by a small number of parameters, which is fitted to the data using a least-squares approach.

Tephra dispersion and attenuation are also estimated using numerical models based on advection–diffusion equations, such as HAZMAP (Macedonio et al. 1988; Barberi et al. 1990), ASHFALL (Hurst and Turner 1999), Tephra 2 (Connor et al. 2001; Bonadonna et al. 2005), or FALL3D (Costa et al. 2006). While these can be used for hazard forecasting as part of a Monte Carlo procedure along with probabilistic models of eruption size and meteorological conditions (Hurst and Smith 2004; Bonadonna et al. 2005; Costa et al. 2009), the inverse problem is less amenable due to difficulty in finding the optimal fit (Connor and Connor 2006). Approaches to inverting the observed tephra dispersal to estimate the eruptive parameters usually use a specified wind profile (e.g., Scollo et al. 2007, 2008; Kratzmann et al. 2010), neglect wind (e.g., Volentik et al. 2010), or apply an exogenously specified average (e.g., Pfeiffer et al. 2005; Johnston et al. 2012), and often fix other parameters as well. The parameters being inverted for are either specified in an experimental design, or optimized in a "one-at-a-time" (Johnston et al. 2012) or downhill simplex scheme (Connor and Connor 2006). There is no objective measure of "best fit"; typically, some form of weighted least-squares error (Costa et al. 2009) is minimized. The results are that the solutions are possibly nonoptimum, not least due to leaving wind out of the design, and can be nonunique (Pfeiffer et al. 2005; Scollo et al. 2007; Kratzmann et al. 2010; Bonasia et al. 2010; Volentik et al. 2010; Johnston et al. 2012) particularly for relatively sparse deposit data, due to the dependencies among the parameters involved.

For modeling tephra fall attenuation from single eruptions, a compromise between the simple tephra attenuation models and the numerical simulations is provided by the class of "semiempirical models." These include the model of Gonzalez-Mellado and De la Cruz-Reyna (2010), which treats the eruptive volume as a parameter, with a wind-based radial dependence term. However, the suggested fitting procedure was via estimated isopachs. Rhoades et al. (2002) examined a data set of multiple eruptions from Taupo Volcano, thus incorporating volume as a variable and developing a linear relationship between the logarithms of thickness and volume, modulated by an elliptical term for wind. The slope and intercept, and the wind-based terms were all estimated along with their variances. The result was used by Bebbington et al. (2008) to produce a probabilistic tephra hazard model for Mt Taranaki.

The advantage of the model of Rhoades et al. (2002) is that it is simple to invert, both to calculate a volume–frequency curve (Bebbington et al. 2008), and to estimate the relative likelihood of a tephra being sourced from different vents (Bebbington and Cronin 2011). The potential disadvantage of this approach is that fitting is done by using linear regression on the logarithm of the thickness. Hence, the variability in the deposited thickness at a given point is assumed to be lognormally distributed. It is not known whether this is the most accurate representation of variability in tephra deposition. Obviously, the distribution must be limited to nonnegative values, but this leaves open many questions regarding its skewness and tail characteristics. For example, the lognormal distribution has a thick tail, implying that very large amounts of overthickening can occur at large distances from the volcano. Other possible alternatives to describe tephra fall attenuation are the Weibull (Bonadonna and Costa 2012) and gamma distributions, which are both capable of having a mode at some positive thickness.

In this paper, we will use the semiempirical model(s) of Gonzalez-Mellado and De la Cruz-Reyna (2010) to estimate the mean tephra thickness to be expected at a given distance and azimuth from an eruption vent, combined with a variety of distributions for the actual thickness given this mean. We will show how the parameters in the semiempirical model and the variance in this "error distribution" can be simultaneously estimated using maximum likelihood methods. In a significant difference from common practice, all our estimation is based on the actual individual tephra thickness measurements, rather than on the derived isopachs. For this purpose, the 1973 Heimaey eruption (Thorarinsson et al. 1973) is used as an example of explosive basaltic (Strombolian) eruption, because it was observed throughout and its published isopach and thickness data are very typical (Self et al. 1974), in being both sparse and not entirely consistent with drawn isopachs.

The remainder of the paper is structured as follows: we will next review the case study data set, that of the 1973

Heimaey eruption (Thorarinsson et al. 1973), and construct a nonparametric estimate of the variability in the deposited thickness. The model(s) are developed in the following section, with the more mathematical details relegated to the Appendix. The results of fitting the models to the Heimaey data are shown in the "Results" section, along with an assessment of how well the various models explain the data and its variation. A sensitivity analysis is presented in section "Sensitivity analyses." The model is extended in section "Multiple lobes and/or vents" to tackle the problem of identifying multiple lobes from possibly multiple sources, illustrated on data from the 1977 Ukinrek Maars eruption. This is followed by discussion.

Data

In order to determine a suitable distribution for the variability in deposited tephra thickness for basaltic explosive eruptions, a data set is required without the complications of multiple lobes or vents, thus the selection of the eruption on 24 January 1973 eruption of Eldfell on Heimaey, Iceland. The tephra dispersal data (Self et al. 1974) were collected from 24 January to 1 February 1973. Winds were blowing predominantly to the northwest and the northeast during the eruption, according to measurements from the Icelandic Meteorological Service at the Storhofdi Lighthouse. While the former wind direction resulted in measurable deposition on land, an estimated 65 % of the tephra deposited under the influence of the westerly winds fell into the sea and were not measured. The resulting single-lobe pattern is ideal for this study. The data consist of observed thicknesses at 36 locations, ranging between 3 and 450 cm, as shown in Fig. 1.

The actual thickness observed at any given point differs from an "ideal" thickness due to small random effects of wind strength and direction, but primarily due to local redistribution of fallen tephra by wind, rain, and slope processes (especially in highly irregular topography). This difference can be termed the "sampling error," which describes the inherent variability of the observations. The absolute error (or residual) at a point i is $A_i = O_i - E_i$, where O_i is the observed thickness at location i, and E_i is the expected thickness at location i. However, a multiplicative error structure is assumed here—such that the size of the error is proportional to the expected thickness. In other words, the focus is the "relative error" $A_i/E_i \geq -1$. For reasons that will become obvious, it is shifted to become nonnegative, and the (shifted) relative error is considered $R_i = A_i/E_i + 1 = O_i/E_i$. Thus, an observation that aligns exactly with the expectation has a relative error of one. Values less than or greater than one indicate under- or over-thickening of the tephra, respectively.

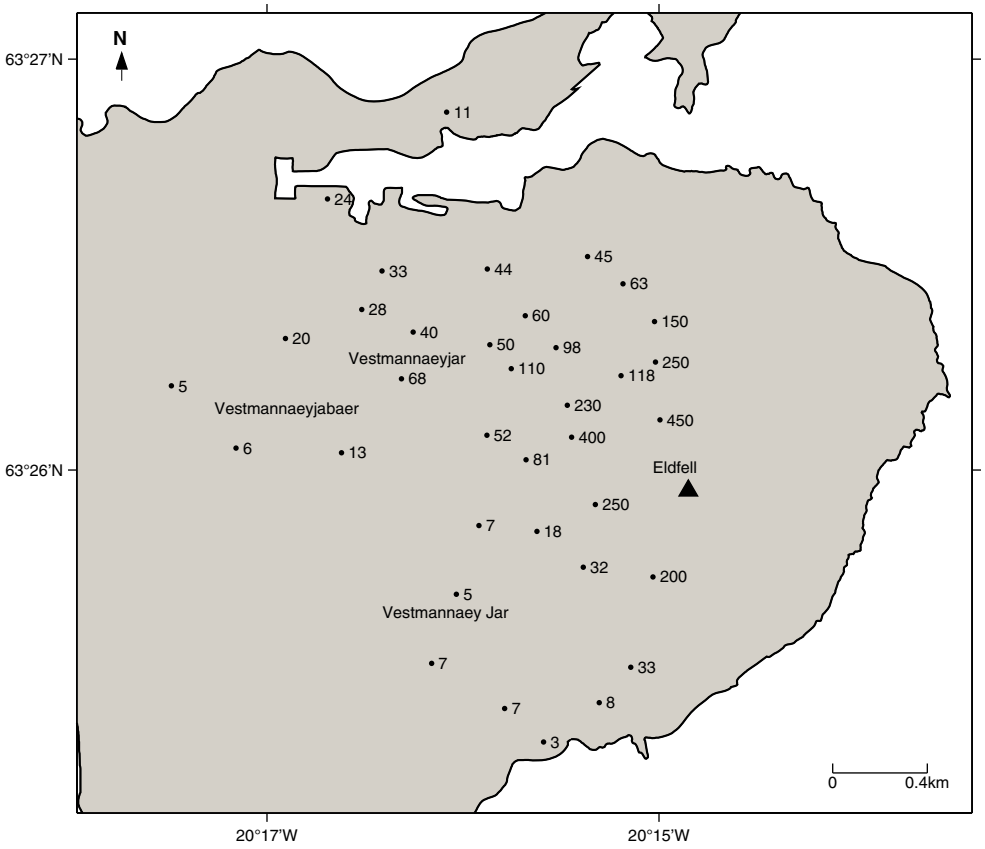

Fig. 1 Heimaey: Observed thickness (in centimeter) and locations. The vent is indicated by the *triangle*

The relative errors are all defined in terms of an expected value that is to be calculated from a parametric model. As the error is thus dependent on the model, and selection amongst multiple models is required, a model independent (nonparametric) of the error distribution is initially estimated in order to discover the candidate parametric distributions that might be suitable.

A leave-one-out cross-validation approach to estimating the expected thickness was applied. The observation at location i is omitted, and a surface is fitted to the remaining 35 data points using a triangulated C_1-continuous interpolating surface. The value of this surface at location i is taken to be E_i. This is repeated for all locations inside the convex hull of the data to obtain relative errors, as shown by the histogram in Fig. 2a. It is clear that the relative sampling error is nonnegative and right-skewed, with a mode less than one. If we denote our relative error by R, then the lognormal

$$f(R) = \frac{1}{R\sqrt{2\pi\sigma^2}} \exp\left[-\frac{(\log R - \mu)^2}{2\sigma^2}\right], \quad (1)$$

Weibull

$$f(R) = \frac{\eta R^{\eta-1}}{\nu^{\eta}} \exp\left[-\left(\frac{R}{\nu}\right)^{\eta}\right], \quad (2)$$

and gamma

$$f(R) = \frac{R^{\kappa-1}}{\omega^{\kappa}\Gamma(\kappa)} \exp\left(\frac{-R}{\omega}\right) \quad (3)$$

distributions are good exemplars of distributions that can be used to model such errors. All have a location parameter (μ, ν, ω) and a shape parameter (σ, η, κ). As can be seen from (1) to (3), they differ mainly in the rate at which the tail decays. The gamma decays much more rapidly than the lognormal, and the Weibull may decay faster or slower than the gamma, depending on the value of the shape parameter η. Fitting these distributions to the nonparametric relative errors via maximum likelihood estimation produces the densities superimposed on the data histogram in Fig. 2a.

The lognormal density is less faithful to the data than the other two candidates, due primarily to the righthand tail of the data not being thick enough, and this is quantified more clearly in Fig. 2b. The maximum distance between the data (the step function) and the curve is the Kolmogorov–Smirnov statistic for the distance between distributions, with values of 0.156, 0.122, and 0.124 for the lognormal, Weibull, and gamma distributions, respectively. While none of these are large enough (> 0.264) to reject the distribution at the 5 % significance level, they do indicate that the Weibull and gamma distributions both fit the data well, and the lognormal slightly less well.

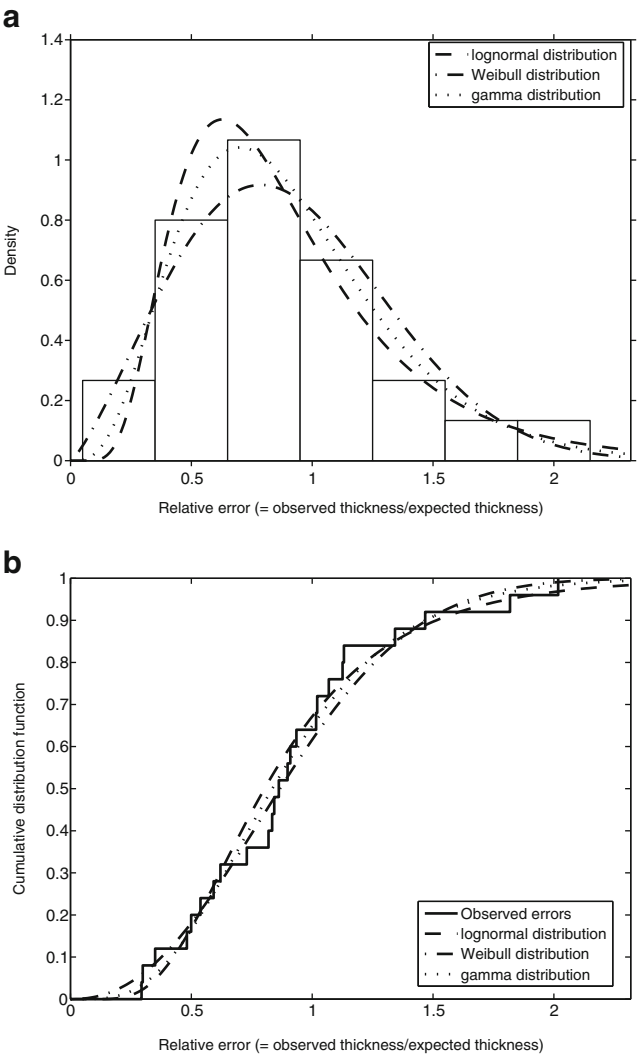

Fig. 2 Nonparametric relative sampling error. **a** Density. **b** Distribution

Methodology

The nonparametric relative errors have been shown to be consistent with the Weibull and gamma, and perhaps lognormal, distributions. Hence, these error distributions were embedded in the framework of a tephra dispersal model. For the reasons outlined in the "intro" section, an empirical model is required that has the facility to include possible wind effect. Since the Rhoades et al. (2002) model assumes a lognormal error distribution, which may not be the best description, the model of Gonzalez-Mellado and De la Cruz-Reyna (2010) is preferred here.

The basic form of the Gonzalez-Mellado and De la Cruz-Reyna (2010) model is that the expected tephra fall deposit thickness is the product of a power-law decay with distance (Bonadonna and Houghton 2005) and a noncircular

term based on wind direction. A power-law decay with distance was preferred to an exponential primarily because it fits well in both the near and far field. It has also been shown that a simple exponential decay may not well describe well-preserved tephra deposits, due to distal ash settling differently (Sparks et al. 1992; Rose 1993). Using the three exponential segments necessary to model accurately the thinning of well-preserved deposits (Bonadonna and Houghton 2005) is also undesirable, because it would add another four parameters to the estimation problem.

The attenuation relation by Gonzalez-Mellado and De la Cruz-Reyna (2010) is

$$T(r, U, \theta) = \gamma \exp\left[-\beta U r(1 - \cos\theta)\right] r^{-\alpha}, \tag{4}$$

where T is the tephra thickness (in centimeter) at a distance from the vent r (in kilometer) in direction θ relative to the wind direction. If the supposed wind direction is given by ϕ, and that the direction from the vent to the deposit location is ξ (both measured in degrees anticlockwise from East), then $\theta = \xi$ - ϕ, and (4) becomes

$$T(r, \xi) = \gamma \exp\{-\beta U r[1 - \cos(\xi - \phi)]\} r^{-\alpha} \tag{5}$$

Note that the wind direction ϕ and speed U (km h^{-1}) are considered as the mean (with respect to the eruption rate) values of the predominant wind, and as such will be estimated from the data (the left-hand side of the equation). The other parameters to be estimated are α, β and γ. The latter is the expected thickness at 1 km from the vent along the dispersal axis, which is a proxy for the eruption size. The dimensionless attenuation parameter α is nonnegative, and β is inversely related to the diffusion coefficient, and thus can be regarded as a proxy for the grain-size distribution. However, there is an identifiability issue, in that βU cannot be separately estimated, and so βU is considered as a single variable, reducing the number of parameters to be estimated to four. Moreover, βU (along with ϕ) is also a nuisance parameter, i.e., one that may or may not be present in the model. If there is no significant wind, then $U = 0$ and (5) reduces to

$$T(r, \xi) = \gamma r^{-\alpha}, \tag{6}$$

with only two parameters to be estimated.

Gonzalez-Mellado and De la Cruz-Reyna (2010) fitted their model to isopach data, thus avoiding the question of sampling error. However, the actual observed tephra thicknesses and locations are used in our formulation, rather than isopachs, and thus sampling error must be included in our fitting. By incorporating an error distribution, the model can be fitted using standard statistical maximum likelihood estimation (MLE) methods. This avoids the necessity of choosing a weighting scheme in the least-squares minimization procedure. The choice of such a weighting scheme depends on the estimated uncertainties (Costa et al. 2009) and can strongly affect the results. In effect, the MLE estimation treats the uncertainties explicitly, rather than approximately.

The error distributions are incorporated by treating the tephra thickness formula (5) or (6) as a link function giving the mean of the thickness distribution at the location (r, ξ). The shape parameter of the distribution (σ for the lognormal, η for the Weibull, κ for the gamma) becomes an additional parameter to be estimated. The likelihood formulae are derived in the Appendix. In each case, we see that the coefficient of variation (standard deviation divided by mean) is a function solely of the shape parameter. In other words, the coefficient of variation is a constant in all directions and at all distances, which is exactly the multiplicative error structure we require.

Two baseline models (with and without wind) and three error distributions makes for a total of six models to be fitted. This leaves the question of which model best describes the data. As all the error distributions have the same number of parameters, this can be decided on the basis of the likelihood. Model (6) is nested within the model (5), and so the model with more parameters can be justified using a likelihood ratio test. A shorthand for this is the Akaike Information Criterion (Akaike 1977):

$$\mathrm{AIC} = 2p - 2\log L, \tag{7}$$

where p is the number of parameters, and $\log L$ the log likelihood. Smaller Akaike Information Criterions (AICs) indicate better models, with the effect of additional parameters being compensated for in order to avoid over-fitting.

Results

Table 1 shows the estimated parameters from fitting each of the six possible models to the Heimaey tephra thickness data. To allow the shape parameters of the three error distributions to be meaningfully compared, they have been converted into a coefficient of variation (CV, the standard deviation divided by the mean), using Eqs. 12, 14, and 16 given in the Appendix. We see that the estimated parameters are consistent for all distributions. In particular, the estimated wind direction ϕ is approximately NNW, in agreement with the meteorological data (Self et al. 1974).

The Weibull distribution has the smallest AIC, indicating that it is the best of the three distributions, but the gamma distribution is not significantly worse. However, the difference in AICs is sufficient to reject the lognormal distribution as a description of the sampling error. Moreover, the lognormal distribution systematically overestimates the volume of the eruption (γ) with respect to the other two distributions.

Table 1 Estimated parameters of the models

Baseline model	Parameter	Error distribution		
		lognormal	Weibull	gamma
(6)	γ	54.0	48.4	48.7
	α	2.00	1.97	1.97
	CV	1.18	0.70	0.78
	$\log L$	−179.4	−175.5	−176.3
	AIC	364.8	357.0	358.5
(5)	γ	83.8	71.0	76.0
	βU	1.42	1.48	1.43
	ϕ	114.1	125.3	119.2
	α	1.61	1.88	1.75
	CV	0.59	0.45	0.49
	$\log L$	−160.1	−157.0	−157.9
	AIC	330.2	324.0	325.7

It also has the highest CV, indicating a poorer absolute fit. Note that the CV decreases for all the error distributions with the introduction of wind effects. There is definitely an improvement from the model (6) without wind, compared to the model (5) incorporating wind. The chi-squared (2 degrees of freedom) statistic of twice the difference in the loglikelihood ratios is significant for all three error distributions, with P values less than 10^{-8} indicating that the model fit is significantly improved by including wind effects.

The AIC and likelihood ratio test tell us which model is better, but the question of whether the model is a good description of the data can only be answered by residual analysis, i.e., by examining the discrepancy between the data and the model. For a first visual inspection, Fig. 3 shows the residual error (observation divided by the expected mean from the model) at each observation location. The means and standard deviations of the residual errors are calculated in Table 2. We see that the residuals are much closer to one (smaller standard deviation) under the model (5). The lognormal overestimates thicknesses (the mean residual, or ratio of observed to estimated, is less than one), for reasons discussed above, while the Weibull and the gamma error distributions appear to be unbiased.

Although some of the residuals from our models are large, the aim is to explicitly quantify this variation.

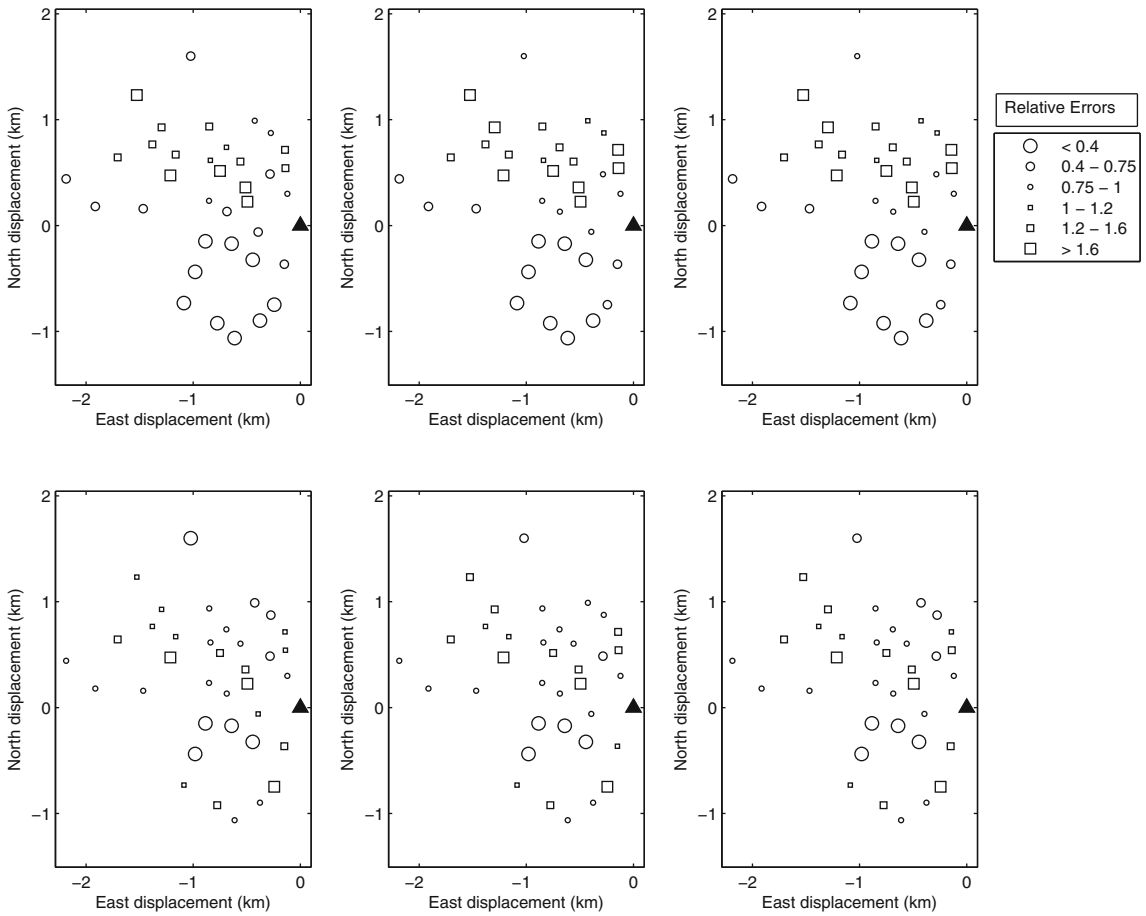

Fig. 3 Relative errors. The *top row* is the model (6) without wind; the *bottom row*, the model (5) with wind. The *columns* are for the lognormal, Weibull, and gamma error distributions, reading *left* to *right*. Displacements are relative to the vent location, indicated by the *triangle*

Table 2 Residual error statistics

Baseline model	Error distribution	Mean	SD
(6)	lognormal	0.899	0.599
	Weibull	1.004	0.669
	gamma	1.000	0.666
(5)	lognormal	0.978	0.461
	Weibull	1.001	0.458
	gamma	1.000	0.463

Whether the residuals are incompatible with the model can be evaluated by obtaining confidence bounds via Monte Carlo simulation. This uses repeated random sampling from the model with the estimated parameters to simulate possible thicknesses consistent with the model at each location. Figure 4 shows the ratio between the simulated and observed thicknesses. A perfect fit is given by the horizontal line, which can be compared with the 90 % point-wise coverage band. For the model (6) without wind, there is a systematic trend with the ratio decreasing with observed thickness. This indicates that small thicknesses are being overfitted, and large thicknesses are underfitted. On the other hand, the baseline model (5) does not exhibit this behavior; it also shows generally tighter bounds. All three error distributions exhibit behavior consistent with the data, although it should be noted that the thick tail (producing occasional very large relative residuals) in the lognormal distribution is not being examined by this procedure.

Sensitivity analyses

The fitted model may be sensitive to either parameters or the data. We will investigate the latter by Monte Carlo simulation and refitting. The Heimaey data consist of 36 tephra thicknesses in the fall direction. We randomly delete $N = 3, 6, 12$, or 24 of these measurements and refit the best model (5) with Weibull error distribution. The results are shown in Table 3. We see that the estimates are consistent in that the means vary little for $N \leq 12$, and that the variability increases with decreasing amounts of data (N increasing). Deleting two thirds of the data ($N = 24$) is too much for the model, inducing a tendency to find more eccentric (higher βU) lobes in variable directions. It appears that a number of the simulations retain locations suggesting different fall directions, or possibly more than one such direction, with consequent instability in the other (coupled) parameters. The error distributions in the parameters are reasonably symmetric, apart from α, as would be expected. We

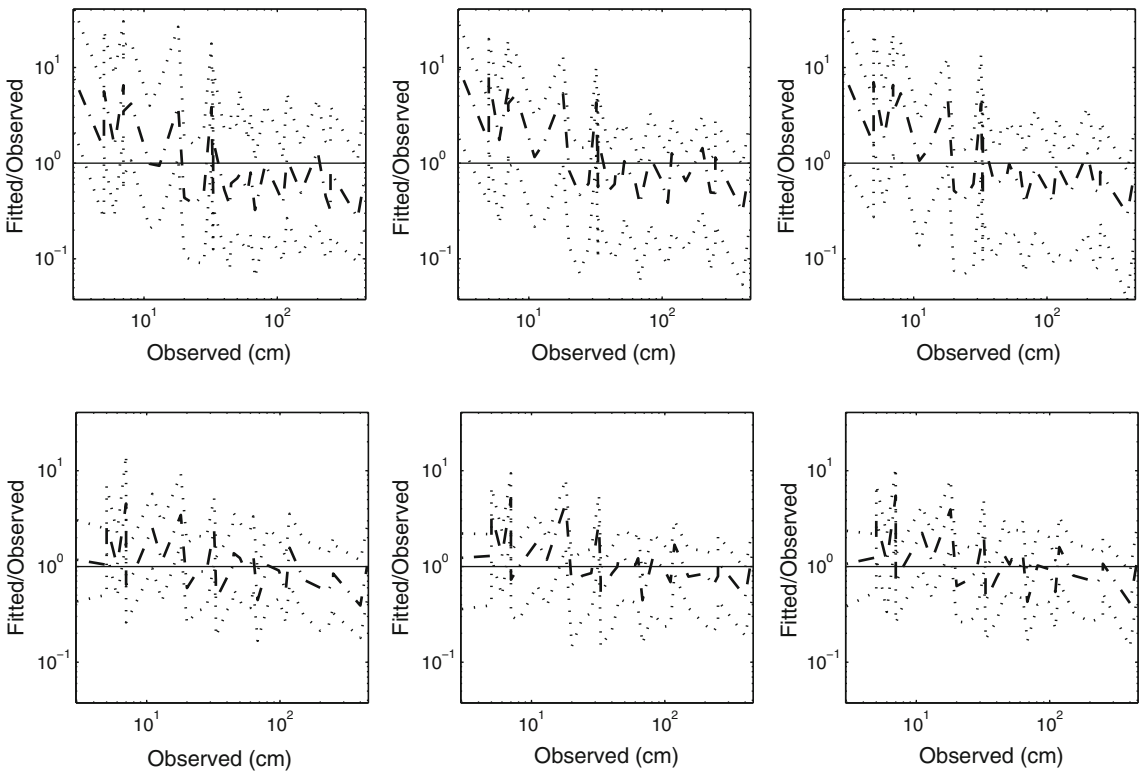

Fig. 4 Monte Carlo residual bounds for tephra thickness. The *top row* is the model (6) without wind; *bottom row*, the model (5) with wind. The *columns* are for the lognormal, Weibull, and gamma error distributions reading *left* to *right*. Medians are shown by the *dashed lines*, 90 % bounds by the *dotted lines*

Table 3 Parameter estimates for the sensitivity analysis on Heimaey data. Errors are 1σ

No. of data	Parameter			
deleted, N	γ	βU	ϕ	α
3	71.3 ± 2.5	1.48 ± 0.07	125.0 ± 4.3	1.88 ± 0.08
6	71.8 ± 4.6	1.49 ± 0.12	124.8 ± 6.9	1.87 ± 0.14
12	72.2 ± 6.0	1.51 ± 0.19	125.9 ± 9.4	1.88 ± 0.19
24	81.4 ± 22.1	1.84 ± 1.04	124.0 ± 19.2	1.85 ± 0.44

can conclude that the model is robust to the amount of data, provided that the data represent the fall pattern correctly; as ever, the garbage-in-garbage-out principle applies.

The sensitivity to the individual parameters is investigated following an idea analogous to that of Scollo et al. (2008). Starting at the optimum solution, we vary each parameter, one at a time, in the best model of (5) with Weibull error distribution. Figure 5 shows the resulting likelihoods, demonstrating that the parameter values are robustly estimated.

Multiple lobes and/or vents

The statistical model readily lends itself to investigation of prehistorical eruptions, allowing us to identify multiple lobes, vents, and eruptions through a mixture framework. In order to demonstrate this, we will briefly analyze the tephra dispersal from the Ukinrek Maars eruption of March and April 1977.

We will suppose that we have m vents, and that the ith vent has n_i components (lobes). The model (4) to prescribe the thickness at a given location then becomes

$$T(r_1, \ldots, r_m, U, \theta_1, \ldots, \theta_m) = \gamma \sum_{i=1}^{m} \sum_{j=1}^{n_i} P_{i,j} \exp\left[-\{\beta U\}_{i,j} r_i (1 - \cos\theta_i)\right] r_i^{-\alpha_{i,j}}, \quad (8)$$

where (r_i, θ_i) is the distance and azimuth (relative to the prevailing wind direction) to the location from the ith vent, and each component has its own α and βU parameters.

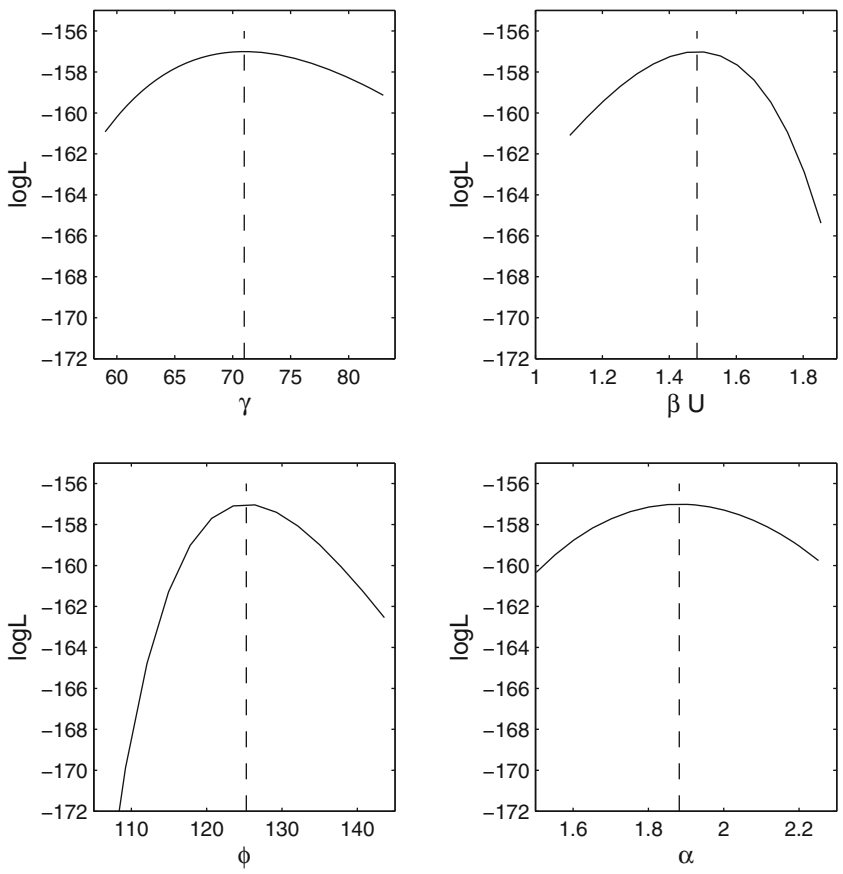

Fig. 5 Sensitivity analysis on the estimated parameters. The maximum likelihood estimates are shown by the *dashed lines*

There is only one γ as the differing sizes of the components are identified through the presence of the mixing distribution $P_{i,j}$, where $\sum_i \sum_j P_{i,j} = 1$. This is equivalent to summing over components with $\gamma_{i,j} = \gamma P_{i,j}$. The models can then be fitted to the data using maximum likelihood, in a minor elaboration of the technique described above.

The tephra thickness data shown in Fig. 6 are taken from Self et al. (1980). Note that we have deleted one thickness measurement of 37 cm approximately 1 km southeast of the East Maar, as it is the only measurement from that described and partly sketched southerly tephra lobe in Self et al. (1980). It is not possible to fit a component with four parameters to a single observation. High-level winds distributing fine tephra to distal areas were apparently not related to the proximal tephra distribution which was controlled only by the low-level winds under 2 km of altitude (Kienle et al. 1980). The West Maar erupted first (30–31 March 1977), with two tephra fall units directed to the SE and SW, overlain by surge deposits, which are thickest on the WSW edge of the crater (Kienle et al. 1980). The map of the deposits is in Self et al. (1980), which includes a slightly different chronology to that in Kienle et al. (1980). The eruption of the East Maar probably began on 1 April (Self et al. 1980), with tephra fallout to the NNE and NNW, with further eruptions on 5 April dispersing tephra to the NW and N. Later, Strombolian phases of eruptions from 7–9 April produced tephra fall lobes to the NW, E, and SSE (Kienle et al. 1980; Self et al. 1980). So, in mixture model terms, the source and direction of the observed components are

West Maar

W1: SE (fall)
W2: SW-WSW (surge plus fall)

East Maar

E1: NNE (fall 2 April)
E2: NW-NNW (fall 1 April, 5 April, and 7–9 April)
E3: WNW (surges throughout eruption)
E4: E (7–9 April)
E5: SSE (7–9 April)

As we have no useable data between SW and ESE, we expect that we will be unable to detect components W1, W2, and E5. Hence, we will limit ourselves to checking for, at most, four components.

Recall that the number of parameters in the distribution is $4N_C$, where N_C is the number of components. This is too many to estimate from the 24 data available (Fig. 6). Hence, we will adopt the earlier idea of fitting a surface to the observed data using a triangulated C_1-continuous interpolating surface, overlaying a grid (at a spacing of 0.25 km) and using the interpolated thicknesses at the grid points (see Fig. 6) as our fitting data. Note that we restrict the grid within the convex hull of the observed data to avoid

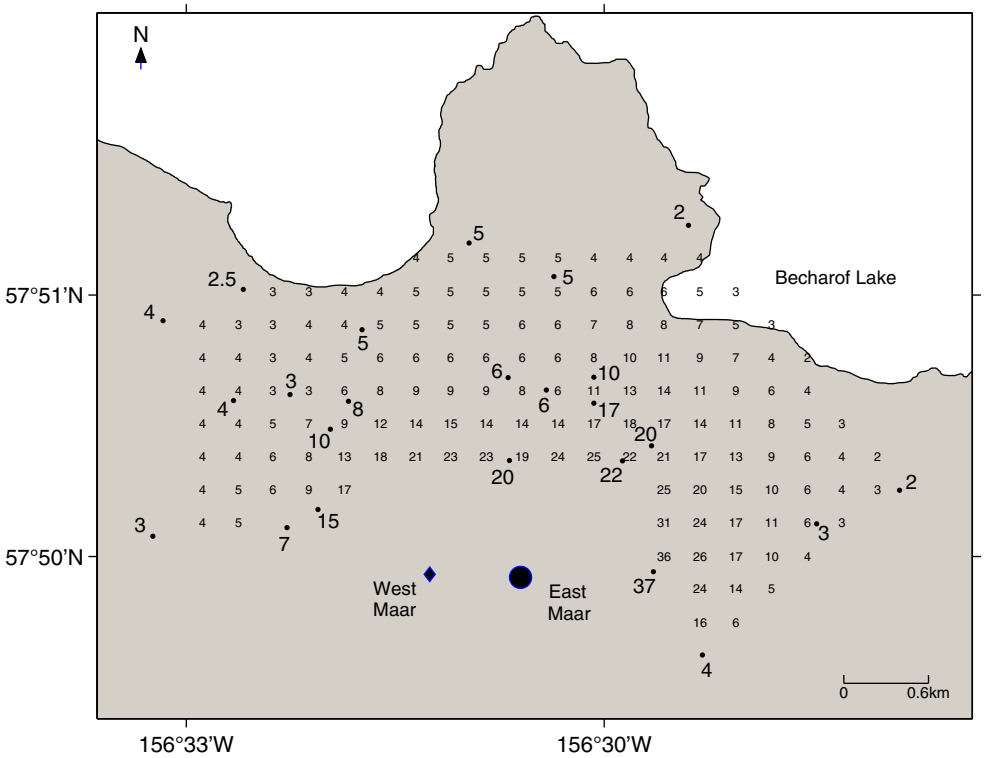

Fig. 6 Ukinrek Maars: Observed thickness (in centimeter) and locations are in large type. Interpolated thicknesses (see text) are in small type. The vents are indicated

extrapolation. This results in c. 150 data, enough to fit the required models.

For the purposes of illustration, we will only present the Weibull error distribution results. The lognormal has already been shown to fit poorly, and while the gamma distribution is a viable alternative for one or two components, it does increasingly poorly relative to the Weibull as the number of components increases. This is understandable, as the thinner tail of the Weibull better describes the reduced sampling variation as excess thicknesses are ascribed to multiple components. Hence, the preferred model, as identified by AIC, will give the number of components (on each Maar). As the East Maar is approximately 16 times the volume of the West Maar (Kienle et al. 1980), we have required at least one component on the East Maar.

The results are shown in Table 4. The best model is clearly that with one component on West Maar (S), and three on East Maar (E, NE and NNW), the last three of which correspond quite closely to the sought-after E4, E1, and E2, respectively. The West Maar component appears to have (correctly) identified the aggregation of W1 and W2 from the scattering opposite to the dispersal axis. This will have been overlaid with E3. The remaining parameter estimates are given in Table 5, although we will restrict further comment to the preferred 1 West/3 East components model, which is illustrated in Fig. 7. All the models assign a minimum weighting of 65 % to the East Maar, while the preferred model assigns 80 % weight to the East Maar. This volume apportioning is consistent with the relative sizes of the two maars and with the fact that the bulk of activity was observed from the latterly erupting East maar (Kienle et al. 1980). The decay with distance (α) and the eccentricity (βU) indicate a wide proximal fall from the West maar, while the East maar contributes two narrower falls (E4 and E1) and a smaller wide deposit slowly thinning with distance (E2). Again, these are in excellent agreement with observations (Kienle et al. 1980, Self et al. 1980). The residual plot for the best fitting model is shown in Fig. 8; there appear to be no systematic patterns.

Discussion

We have considered only the tephra thickness, as this is the most common directly measured quantity. In many respects, particularly the risk to built structures, the tephra loading can be a more important measure. Often, thickness is converted into loading by assuming an average particle bulk density and packing density; measured values are often in the range of 1,000 to 1,400 kg/m^3 (Cronin et al. 1998). It is possible that a method similar to that above could be developed to model tephra loading directly, provided that an attenuation model can be formulated.

Gonzalez-Mellado and De la Cruz-Reyna (2010) derived a number of empirical relationships based on fitting their model (4) to 14 well-documented eruptions. In particular, they found that

$$\alpha = 2.535 - 0.051H, \tag{9}$$

giving an estimate of H, the height (in kilometer) of the eruption column. It should be borne in mind that both α and H have uncertainties associated with them besides those allowed for in the regression analysis, and so this relation is an approximation at best. Of course, the attenuation parameter α is also a function of total grain-size distribution, which is linked to column height. A second relationship between β and the column height,

$$\frac{1}{2\beta} = \begin{cases} 114.407 - 4.189H & H < 15.5, \\ -770.17 + 52.822H & H \geq 15.5, \end{cases} \tag{10}$$

which might otherwise allow us to separate the wind speed U from βU, appears to be an artifact of the inclusion of the Pinatubo-2 eruption, with its column height of 43 km. Without this point, a quadratic regression has an adjusted R^2 of zero, indicating no relationship.

For Heimaey, calculating H from the estimated α via (9), using the example of the Weibull error distribution and baseline model (5) which had the best AIC, yields an estimated column height of $H = 2.44$ km, in line with the observed 2–3 km (Wilson et al. 1978). We note that, in this instance, the

Table 4 Ukinrek models, AICs, and fall directions

Model (no. of components)		AIC	γ	Directions (deg. anticlockwise from E)	
West Maar	East Maar			West Maar	East Maar
0	2	570.0	39.5		216, 39
1	1	538.9	44.8	90	30
0	3	514.5	78.7		27, 158, 96
1	2	498.9	67.0	94	12, 52
2	1	516.2	66.0	89, 42	18
1	3	468.9	74.0	264	12, 52, 113
2	2	477.0	78.3	297, 98	12, 52
0	4	484.9	78.7		15, 157, 99, 55

Table 5 Ukinrek models, estimated parameters

Model (no. of components)		P		βU		α	
West Maar	East Maar	West Maar	East Maar	West Maar	East Maar	West Maar	East Maar
0	2		0.64, 0.36		0.1, 3.7		1.9, 2.3
1	1	0.28	0.72	0.3	1.8	1.5	2.5
0	3		0.46, 0.46, 0.08		1.9, 4.6, 0.9		2.6, 2.9, 0.4
1	2	0.21	0.56, 0.23	0.4	4.8, 5.2	1.6	3.1, 1.7
2	1	0.20, 0.15	0.65	0.4, 10.5	4.0	1.5, 1.0	3.2
1	3	0.20	0.51, 0.21, 0.07	0.2	5.0, 6.1, 0.6	3.2	3.1, 1.7, 0.4
2	2	0.23, 0.06	0.49, 0.21	0.3, 0.6	5.3, 5.6	2.9, 0.3	3.2, 1.7
0	4		0.42, 0.35, 0.13, 0.10		3.4, 4.5, 0.7, 9.9		2.7, 2.7, 1.1, 1.3

particle density is near-uniform across the deposit (mean $\pm$ standard deviation of 2.08 ± 0.29 g/cm^3 from 99 measurements). Hence, the isopachs are a constant function of the isopleths which are usually used to estimate column height.

As the Heimaey eruption was observed, we have the average wind velocity to the NW, which seems to have been on the order of 50 km/h (Self et al. 1974). From the estimated $\beta U = 1.48$, this gives a value of $\beta = 0.03$ and, thus, an "effective diffusion coefficient" (Gonzalez-Mellado and De la Cruz-Reyna 2010) $D = 17$ km^2/h $= 4{,}700$ m^2/s, which appears reasonable.

The relation (9) appears to break down for the Ukinrek model with α's greater than 2.535 (negative column height), or small enough ($\alpha = 0.3$) to correspond to a 44-km column height. The observed column heights (Kienle et al. 1980) of 6.5 km (West Maar) and 3.5 km (East Maar) would require α's of 2.2 and 2.4, respectively. We note that the less complex models in Table 5 have α's much closer to these ideal values. Thus, the empirical relation (9) appears more likely to be valid where the deposit is a single lobe corresponding to the maximum column height, which are the conditions under which it was derived by Gonzalez-Mellado and De la Cruz-Reyna (2010). The higher βU values observed for some of the components in Table 5 may reflect the generally higher wind velocity environment at Ukinrek, wind shear causing bent-over plumes, or directional control in the individual eruptions.

The diffusion coefficient is also an empirical parameter in such "semianalytical" models such as TEPHRA2 and HAZMAP, "describing complex plume and atmospheric processes not captured in the physical model" (Volentik et al. 2010). Hence, the difference in "physical reality" between physical and statistical models is one of degree rather than a hard boundary. The advantage of the

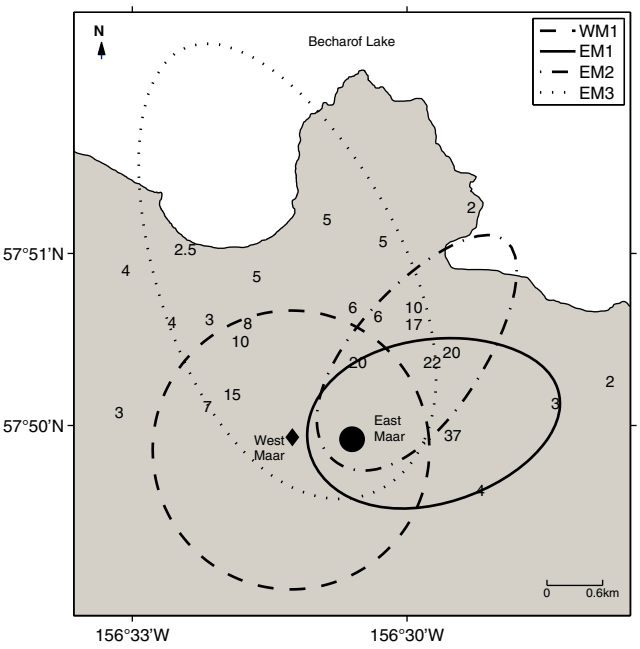

Fig. 7 Ukinrek Maars: The 3-cm isocontours for each component are shown. WM1 is the West Maar component, while the East Maar components are denoted EM1–EM3, as detailed in Tables 4 and 5. Observed thickness (in centimeter) and locations are also shown. The vents are indicated

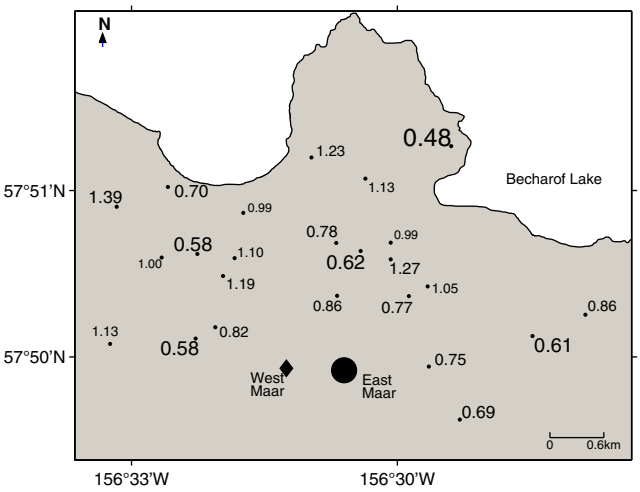

Fig. 8 Ukinrek: Relative errors at measurement locations for the 1 West/3 East components model. The text is scaled by size of error. The vents are indicated

statistical model is that there is an objective, consistent method of parameter estimation through maximum likelihood. The advantage of the physical model is that "feasible," but perhaps not consistent, estimates of column height and mass eruption rate can be obtained, provided that grain-size information and/or eruption duration is also available.

Heimaey and Ukinrek are typical examples of basaltic systems, scaled appropriately for the typical eruption types occurring in monogenetic volcanic fields. Hence, the lessons from this study can be carried over to reconstruction of parameters of tephra falls in prehistoric eruptions in such fields, after allowance is made for tephra settling and compaction. The successful inferences made from the very sparse (and partially incomplete) thickness data for Ukinrek is particularly encouraging, showing that this approach is applicable to the typical quality of data obtainable through paleo-volcanology studies. In particular, the statistical model for tephra variation provides a platform for maximum likelihood estimation and, hence, the use of penalized fitting criteria such as the AIC, which permits consistent estimation of the number of lobes. While multiple tephra lobes can be inferred in complex multi-event eruption episodes using this method, the order of these cannot be extracted without additional stratigraphic information. On the other hand, we can estimate eruptive parameters including volume and identify statistically the likely sources among multiple eruptive centers (cf. Bebbington and Cronin 2011) and, thus, incorporate this into hazard estimates.

In estimating the actual volume, the fact that the power law produces an infinite thickness at $r = 0$ is an issue. To get around this, we could possibly follow the lead of Rhoades et al. (2002) and replace $r^{-\alpha}$ by $(r + \delta\gamma)^{-\alpha}$, which is dimensionally correct, and gives a finite thickness at $r = 0$, at the price of adding one more parameter to the estimation problem. However, it is easier to simply exclude the area of the crater from calculations following, in effect, the suggestion of Bonadonna and Houghton (2005). Volumes can most easily be calculated by numerical integration of the Eq. 4, using the estimated parameters.

Conclusion

We have shown that a semiempirical model of tephra deposition can be combined with an error distribution to produce a statistical model capable of being fitted to actual measurements rather than isopachs constructed from these measurements. This provides a ready-made inversion formula for the volume of the eruption and the average dispersal axis. In addition, it can be used to forecast the distribution of tephra at locations without data, and it provides an objective measure of goodness of fit to the data.

Applied to the 1973 Heimaey eruption, we were able to decisively reject the model without wind effects. The wind direction obtained with the other model corresponds well with the mean wind direction from the onshore wind that deposited the measured tephra thicknesses. The estimated attenuation parameter indicated a mean column height equal to that observed for the eruption (Wilson et al. 1978).

Elaborating the model further in a mixture framework enables the model to fit multiple lobes and/or vents. Applied to the 1977 Ukinrek Maars eruption, it was able to identify lobes in the correct direction from each vent. This has obvious utility in studying unobserved eruptions with multiple vents.

Acknowledgments The first author (E.K.) is supported by the New Zealand Earthquake Commission and GNS Science. M.B. and S.C. are supported by the New Zealand Natural Hazards Research Platform, project "Living with Volcanic Risk." We thank Christina Magill and an anonymous reviewer for improvements suggested to the original manuscript.

Appendix

Here, we derive the likelihood formulae for the various combinations of model and error distribution. Let T denote the tephra thickness obtained from (5) or (6).

Lognormal distribution

Assume $T \sim$ lognormal (μ_N, σ_N) where μ_N is the location parameter and σ_N is the scale parameter of the conjugate normal distribution. Thus, $\mu_{LN} = \exp\left(\mu_N + \sigma_N^2/2\right)$ and $\sigma_{LN} = \sqrt{\left[\exp\left(\sigma_N^2\right) - 1\right]\exp\left(2\mu_N + \sigma_N^2\right)}$ are the lognormal parameters by definition. Then, $\mu_{LN_i} = T_i(r_i, \xi_i)$ for the ith observation, and so $\mu_{N_i} = \log T_i - \sigma_N^2/2$. Note that the location parameter is no longer a constant, as it varies for each observation.

The loglikelihood function for the complete sample $i = 1, 2, \ldots, n$ is then obtained from (1) as follows:

$$\log L = -\frac{n}{2}\left[\log\left(2\pi\sigma_N^2\right)\right] - \sum_{i=1}^{n}\log T_i - \frac{\sum_{i=1}^{n}\left(\log T_i - \mu_{N_i}\right)^2}{2\sigma_N^2}, \tag{11}$$

and the coefficient of variation is

$$\mathrm{CV} = \frac{\sigma_{LN}}{\mu_{LN}} = \sqrt{\left[\exp\left(\sigma_N^2\right) - 1\right]\exp\left(2\mu_{N_i} + \sigma_N^2\right)}/\exp\left(\mu_{N_i} + \sigma_N^2/2\right) = \sqrt{\exp\left(\sigma_N^2\right) - 1}. \tag{12}$$

Weibull distribution

Assume $T \sim$ Weibull (η, ν) where η is the shape parameter and ν is the scale parameter. Then $\mu_W = \nu\Gamma\,(1 + 1/\eta)$ and $\sigma_W = \nu\sqrt{\Gamma\,(1 + 2/\eta) - \Gamma^2\,(1 + 1/\eta)}$ by definition. Thus, $\mu_{W_i} = T_i(r_i, \xi_i)$ for the ith observation, and $\nu_i = T_i/\,\Gamma(1 + 1/\eta)$. Again, the scale parameter is no longer a constant, as it varies for each observation.

The loglikelihood function for the complete sample $i = 1, 2, \ldots, n$ is then obtained from (2) as follows:

$$\log L = n\log\eta + (\eta - 1)\sum_{i=1}^{n}\log T_i - \eta\sum_{i=1}^{n}\log\nu_i - \sum_{i=1}^{n}\left(\frac{T_i}{\nu_i}\right)^{\eta}, \tag{13}$$

and the coefficient of variation is

$$\mathrm{CV} = \frac{\sigma_W}{\mu_W} = \nu_i\sqrt{\Gamma\,(1 + 2/\eta) - \Gamma^2\,(1 + 1/\eta)}/\,(\nu_i\Gamma(1 + 1/\eta)) = \sqrt{\frac{\Gamma(1 + 2/\eta)}{\Gamma^2(1 + 1/\eta)} - 1}. \tag{14}$$

Gamma distribution

Assume $T \sim$ gamma (κ, ω) where κ is the shape parameter and ω is the scale parameter. Then $\mu_G = \kappa\omega$ and $\sigma_G = \sqrt{\kappa}\omega$ by definition. So, $\mu_{G_i} = T_i(r_i, \xi_i)$ for the ith observation, and $\omega_i = T_i/\kappa$. Again, the scale parameter is no longer a constant.

The loglikelihood function for the complete sample $i = 1, 2, \ldots, n$ is then obtained from (3) as follows:

$$\log L = (\kappa - 1)\sum_{i=1}^{n}\log T_i - \kappa\sum_{i=1}^{n}\log\omega_i - n\log\Gamma(\kappa) - \sum_{i=1}^{n}\frac{T_i}{\omega_i}, \tag{15}$$

and the coefficient of variation is

$$\mathrm{CV} = \frac{\sigma_G}{\mu_G} = \frac{\sqrt{\kappa}\omega_i}{\kappa\omega_i} = \frac{1}{\sqrt{\kappa}}. \tag{16}$$

References

Akaike H (1977) On entropy maximization principle. In: Krishnaiah PR (ed) Applications of statistics. North-Holland, Amsterdam, pp 27–41

Barberi F, Macedonio G, Pareschi MT, Santacroce R (1990) Mapping the tephra fallout risk: an example from Vesuvius, Italy. Nature 344:142–144

Baxter PJ, Ing R, Falk H, French J, Stein GF, Bernstein RS, Merchant JA, Allard J (1981) Mount St. Helens eruptions, May 18 to June 12, 1980: an overview of the acute health impact. J Am Med Assoc 246:2585–2589

Bebbington M, Cronin SJ (2011) Spatio-temporal hazard estimation in the Auckland Volcanic field, New Zealand, with a new event-order model. Bull Volcanol 73:55–72

Bebbington M, Cronin S, Chapman I, Turner M (2008) Quantifying volcanic ash fall hazard to electricity infrastructure. J Volcanol Geotherm Res 177:1055–1062

Bonadonna C, Houghton BF (2005) Total grain-size and volume of tephra-fall deposits. Bull Volcanol 67:441–456

Bonadonna C, Costa A (2012) Estimating the volume of tephra deposits: a new simple strategy. Geology 40:415–418

Bonadonna C, Ernst GGJ, Sparks RSJ (1998) Thickness variations and volume estimates of tephra fall deposits: the importance of particle Reynolds number. J Volcanol Geotherm Res 81:173–187

Bonadonna C, Connor CB, Houghton BF, Connor L, Byrne M, Laing A, Hincks T (2005) Probabilistic modeling of tephra dispersion: hazard assessment of a multi-phase eruption at Tarawera, New Zealand. J Geophys Res 110:B03203

Bonasia R, Macedonio G, Costa A, Mele D, Sulpizio R (2010) Numerical inversion and analysis of tephra fallout deposits from the 472 AD sub-Plinian eruption at Vesuvius (Italy) through a new best-fit procedure. J Volcanol Geotherm Res 189:238–246

Carey S, Sparks RSJ (1986) Quantitative models of the fall and dispersal of tephra from volcanic eruption columns. Bull Volcanol 48:109–125

Connor CB, Hill BE, Winfrey B, Franklin NM, LaFemina PC (2001) Estimation of volcanic hazards from tephra fallout. Nat Haz Rev 2:33–42

Connor LJ, Connor CB (2006) Inversion is the key to dispersion: understanding eruption dynamics buy inverting tephra fallout. In: Mader H et al. (ed) Statistics in volcanology, vol 1: special publications of IAVCEI. Geological Society, London, pp 231–242

Costa A, Macedonio G, Folch A (2006) A three-dimensional Eulerian model for transport and deposition of volcanic ashes. Earth Planet Sci Lett 241:634–647

Costa A, Dell'Erba F, Di Vito MA, Isaia R, Macedonio G, Orsi G, Pfeiffer T (2009) Tephra fallout hazard assessment at the Campi Flegrei caldera (Italy). Bull Volcanol 71:259–273

Cronin SJ, Hedley MJ, Neall VE, Smith G (1998) Agronomic impact of tephra fallout from 1995 and 1996 Ruapehu volcano eruptions, New Zealand. Environ Geol 34:21–30

Fierstein J, Nathenson M (1992) Another look at the calculation of fallout tephra volumes. Bull Volcanol 54:156–167

Gonzalez-Mellado AO, De la Cruz-Reyna S (2010) A simple semi-empirical approach to model thickness of ash-deposits for different eruption scenarios. Nat Haz Earth Syst Sci 10:2241–2257

Heiken G, Murphy M, Hackett W, Scott W (1995) Volcanic hazards on energy infrastructure of the United States. United States Department of Energy, Washington DC, LA-UR 95-1087

Hurst AW, Turner R (1999) Performance of the program ASHFALL for forecasting ashfall during the 1995 and 1996 eruptions of Ruapehu volcano. NZ J Geol Geophys 42:615–622

Hurst T, Smith W (2004) A Monte Carlo methodology for modelling ashfall hazards. J Volcanol Geotherm Res 138:393–403

Johnston EN, Phillips JC, Bonadonna C, Watson IM (2012) Reconstructing the tephra dispersal pattern from the bronze age eruption of Santorini using an advection-diffusion model. Bull Volcanol 74:1485–1507

Kienle J, Kyle PR, Self S, Motyka RJ, Lorenz V (1980) Ukinrek Maars, Alaska, I. April 1977 eruption sequence, petrology and tectonic setting. J Volcanol Geotherm Res 7:11–37

Kratzmann DJ, Carey SN, Fero J, Scasso RA, Naranjo J-A (2010) Simulations of tephra dispersal from the 1991 explosive eruptions of Hudson volcano, Chile. J Volcanol Geotherm Res 190:337–353

Macedonio G, Pareschi MT, Santacroce R (1988) A numerical simulation of the Plinian fall phase of 79 AD eruption of Vesuvius. J Geophys Res 93:14817–14827

Miller TP, Casadevall TJ (2000) Volcanic ash hazards to aviation. In: Sigurdsson H (ed) Encyclopedia of volcanoes. Academic, San Diego, pp 915–930

Pfeiffer T, Costa A, Macedonio G (2005) A model for the numerical simulation of tephra fall deposits. J Volcanol Geotherm Res 140:273–294

Pyle DM (1989) The thickness, volume and grain size of tephra fall deposits. Bull Volcanol 51:1–15

Pyle DM (2000) Sizes of volcanic eruptions. In: Sigurdsson H, et al. (eds) Encyclopedia of volcanoes. Academic, San Diego, pp 263–269

Rhoades DA, Dowrick DJ, Wilson CJN (2002) Volcanic hazard in New Zealand: scaling and attenuation relations for tephra fall deposits from Taupo volcano. Nat Hazards 26:147–174

Rose WI (1993) Comment on 'another look at the calculation of fallout tephra volumes' by Judy Fierstein and Manuel Nathenson. Bull Volcanol 55:372–374

Scollo S, Del Carlo P, Coltelli M (2007) Tephra fallout of 2001 Etna flank eruption: analysis of the deposit and plume dispersion. J Volcanol Geotherm Res 160:147–164

Scollo S, Tarantola S, Bonadonna C, Coltelli M, Saltelli A (2008) Sensitivity analysis and uncertainty estimation for tephra dispersal models. J Geophys Res 113:B06202

Self S, Sparks RSJ, Booth B, Walker GPL (1974) The 1973 Heimaey Strombolian scoria deposit, Iceland. Geol Mag 111:539–548

Self S, Kienle J, Huot J-P (1980) Ukinrek Maars, Alaska, II. Deposits and formation of the 1977 craters. J Volcanol Geotherm Res 7:39–65

Sparks RSJ (1986) The dimension and dynamics of volcanic eruption columns. J Volcanol Geotherm Res 48:13–15

Sparks RSJ, Bursik MI, Ablay GJ, Thomas RME, Carey SN (1992) Sedimentation of tephra by volcanic plumes. 2: controls on thickness and grain-size variations of tephra fall deposits. Bull Volcanol 54:685–695

Sparks RSJ, Bursik M, Carey SN, Gilbert JS, Glaze LS, Sigurdsson H, Woods AW (1997) Volcanic plumes. Wiley, Chichester, pp 574

Stewart C, Johnston DM, Leonard G, Horwell C, Thordarsson T, Cronin SJ (2006) Contamination of water supplies by volcanic ashfall: a literature review and simple impact modelling. J Volcanol Geotherm Res 158:296–306

Sulpizio R (2005) Three empirical methods for the calculation of distal volume of tephra-fall deposits. J Volcanol Geotherm Res 145(3–4):315–33

Thorarinsson S, Steinthorsson S, Einarsson Th, Kristmannsdottir H, Oskarsson N (1973) The eruption on Heimaey, Iceland. Nature 241:372–375

Volentik ACM, Bonadonna C, Connor CB, Connor LJ, Rosi M (2010) Modeling tephra dispersal in absence of wind: insights from the climatic phase of the 2450 BP Plinian eruption of Pululagua volcano (Ecuador). J Volcanol Geotherm Res 193:117–136

Wilson L, Sparks RSJ, Huang TC, Watkins ND (1978) The control of volcanic column heights by eruption energetics and dynamics. J Geophys Res 83:1829–1836